Geophysical Prospecting **41**, 1009–1031, 1993

DEPTH IMAGING OF OFFSET VERTICAL SEISMIC PROFILE DATA[1]

LASSE AMUNDSEN,[2] BØRGE ARNTSEN[2] and RUNE MITTET[3]

ABSTRACT

AMUNDSEN, L., ARNTSEN, B. and MITTET, R. 1993. Depth imaging of offset vertical seismic profile data. *Geophysical Prospecting* **41**, 1009–1031.

Depth migration consists of two different steps: wavefield extrapolation and imaging. The wave propagation is firmly founded on a mathematical frame-work, and is simulated by solving different types of wave equations, dependent on the physical model under investigation. In contrast, the imaging part of migration is usually based on *ad hoc* 'principles', rather than on a physical model with an associated mathematical expression. The imaging is usually performed using the U/D concept of Claerbout (1971), which states that reflectors exist at points in the subsurface where the first arrival of the downgoing wave is time-coincident with the upgoing wave.

Inversion can, as with migration, be divided into the two steps of wavefield extrapolation and imaging. In contrast to the imaging principle in migration, imaging in inversion follows from the mathematical formulation of the problem. The image with respect to the bulk modulus (or velocity) perturbations is proportional to the correlation between the time derivatives of a forward-propagated field and a backward-propagated residual field (Lailly 1984; Tarantola 1984).

We assume a physical model in which the wave propagation is governed by the 2D acoustic wave equation. The wave equation is solved numerically using an efficient finite-difference scheme, making simulations in realistically sized models feasible. The two imaging concepts of migration and inversion are tested and compared in depth imaging from a synthetic offset vertical seismic profile section. In order to test the velocity sensitivity of the algorithms, two erroneous input velocity models are tested. We find that the algorithm founded on inverse theory is less sensitive to velocity errors than depth migration using the more *ad hoc* U/D imaging principle.

INTRODUCTION

In recent years, offset vertical seismic profile (VSP) data have frequently been used to map the subsurface away from the borehole. The mapping may be achieved

[1] Paper presented at the 49th EAEG meeting, Belgrade, June 1987. Received February 1991, revision accepted June 1993.

[2] Statoil Research Center, Postuttak, N-7004 Trondheim, Norway, Formerly: IKU Petroleum Research A/S.

[3] IKU Petroleum Research A/S, N-7034 Trondheim, Norway.

through migration. Extrapolation methods for migration using VSP data have mainly been based on the Kirchhoff integral (Wiggins 1984; Wiggins and Levander 1984; Keho 1984; Kohler and Koenig 1986; Dai and Kuo 1986; Hu and McMechan 1986; Dillon 1988; Dillon, Ahmed and Roberts 1988) or the finite-difference technique (Chang and McMechan 1986; Whitmore and Lines 1986). Miller, Oristaglio and Beylkin (1987) (see also Beylkin and Burridge 1990) presented generalized Radon transform (GRT) migration, which can handle any configuration of sources and geophones. GRT migration may be viewed as a weighted version of a generalized Kirchhoff migration technique (Dillon 1990).

The reverse time finite-difference migration algorithms which have been in use are based on time-coincidence in space of upgoing and downgoing waves, and share the common idea that the downgoing source wavefield and the upgoing (reflected) receiver wavefield can be extrapolated independently. Chang and McMechan (1986) use the excitation-time imaging condition (each point in the image space has its own image time). Whitmore and Lines (1986) compute the reflectivity by correlating an incident and a reflected field normalized by the square of the incident field. The incident field is modelled using the acoustic wave equation with a constant specific impedance. The reflected field is produced by backward time propagation of the reflected part of the VSP data as a source in the wave equation with constant impedance.

The mapping of reflectors in the subsurface from time measurements obtained in seismic experiments is an inverse problem. Therefore, it is possible, in the mapping, to utilize elements from the relationship between depth migration and non-linear inversion. Inversion can, as with migration, be divided into two different steps of wavefield extrapolation and imaging (Lailly 1984; Tarantola 1984). Considerable research has been concentrated on the wavefield extrapolation step of migration, and it relates closely to the extrapolation step of inversion. However, the imaging step of migration is usually based on *ad hoc* 'principles', whereas the imaging step deduced from inversion follows from the formulation of the problem. It may therefore be interesting to replace the *ad hoc* imaging principles of migration with the better, theoretically founded, imaging equations of inversion.

The main objective of this paper is to examine the sensitivity of the imaging algorithm rooted in the theory of acoustic inversion to velocity errors in the background velocity model. We generate synthetic VSP data from a rather complicated geological structure and perturb the true velocity model in the target zone in two different ways to study the effects of velocity errors. We also compare this imaging concept to imaging in migration, that is, full wavefield extrapolation followed by application of the U/D imaging concept of Claerbout (1971). Both algorithms require a background velocity model, or 'macromodel' (Berkhout 1986), above the target zone.

The implementation of the migration algorithm based on the U/D imaging concept differs from the algorithms that have been published previously. In contrast to, for instance, Whitmore and Lines (1986), who perform two modelling operations in the depth imaging, we extrapolate the field at the receivers backwards in time, and at each lateral position we separate the wavefield into upgoing and downgoing

waves by a wavenumber–frequency filtering technique. From a computational point of view, this imaging only requires one wavefield simulation. Observe that the wavefield extrapolation requires, in principle, two boundary conditions.

This paper is divided into six sections. We first introduce the notation used. The second section briefly reviews the forward modelling equations. Sections three and four consider depth imaging based on depth migration and inversion, respectively. In the two last sections the numerical results and conclusions are given. For completeness, we derive several well-known equations in the appendices. In Appendix A the acoustic equations, the properties of the Green's function, and closed-form integral solutions of the scalar wave equation in terms of the Green's function, are listed. In Appendix B we summarize some elements of the inversion theory given by Lailly (1984) and Tarantola (1984).

NOTATION

Let $\mathbf{x}$ be a shorthand notation for the Cartesian coordinates. In a seismic experiment $\mathbf{x}_s$ denotes a shot position, and ξ denotes a receiver position on a surface S. We will distinguish between the two different surface integrals $\oint_S$ and $\int_S$. The first integral always designates a *closed* surface integral surrounding a volume V. The second integral designates an integral along a part of the surface S.

We use Einstein's summation convention for the repeated Latin indices i and j. The index i may be 1, 2 or 3 representing the orthogonal coordinate directions x_1, x_2 and x_3 (x, y and z), respectively. A spatial derivative is denoted ∂_i and a temporal derivative ∂_t. Then, when n_i is component i of an outward-pointing unit vector orthogonal to the surface S bounding the volume V, normal derivative of a field $\psi(\xi, t)$ on S is denoted by $n_i\, \partial_i^{\xi} \psi(\xi, t)$. We use the shorthand notation ∂_i^{ξ} for indicating that the derivative of a field is to be taken with respect to the coordinate ξ on S, that is

$$n_i\, \partial_i^{\xi} \psi(\xi, t) = n_i [\partial_i \psi(\mathbf{x}, t)]_{\mathbf{x}=\xi}.$$

FORWARD MODELLING

We consider 2D wave propagation in a 2D acoustic medium characterized by the density $\rho(\mathbf{x})$ and the bulk modulus $M(\mathbf{x})$. The P-wave velocity is $c(\mathbf{x}) = \sqrt{M(\mathbf{x})/\rho(\mathbf{x})}$. Given the source $f(\mathbf{x}, t)$, the pressure field $p(\mathbf{x}, t)$ obeys the acoustic wave equation ((A2a) in Appendix A)

$$\left[\frac{1}{M(\mathbf{x})}\, \partial_t^2 - \partial_i \frac{1}{\rho(\mathbf{x})}\, \partial_i\right] p(\mathbf{x}, t) = f(\mathbf{x}, t), \tag{1}$$

with given initial and boundary conditions. In a forward simulation of a seismic experiment the initial conditions are zero (A3), and the pressure field is zero at the earth's surface. We assume that the source term corresponds to an explosive point

source at location $\mathbf{x}_s$ with time function $s(t)$, that is

$$f(\mathbf{x}, t) = -\partial_i \frac{1}{\rho(\mathbf{x})} \partial_i \delta(\mathbf{x} - \mathbf{x}_s) s(t). \tag{2}$$

From (A15) it follows that the integral representation for the forward-propagated pressure, assuming homogeneous boundary conditions, can be expressed in terms of the Green's function g as

$$p(\mathbf{x}, t) = \int_V \mathrm{d}V(\mathbf{x}') g(\mathbf{x}, t \,|\, \mathbf{x}', 0) * f(\mathbf{x}', t), \tag{3}$$

where the time convolution ($*$) is defined in (A14). The equation (A5) determining the Green's function is given in Appendix A. Equations (1) and (3) both give the solution of the forward problem.

The integral representation of a differential equation with associated boundary conditions is often more amenable to mathematical manipulations than the differential equation itself. However, we always perform the numerical computations using a finite-difference approximation to the differential equation corresponding to an integral equation. For details of the design of the finite-difference operators, see Holberg (1987).

Depth Imaging Based on Depth Migration

The depth-migration problem is solved in two steps. First we extrapolate the measured wavefield at the receivers into the medium. Then we image the extrapolated field at every point in a target zone. The extrapolated field is obtained by running the finite-difference algorithm with the time-reversed field as sources at the receiver locations. The imaging concept is intuitive, and states that reflectors exist at points in the subsurface where the first arrival of the downgoing wave is time-coincident with the upgoing wave (Claerbout 1971). The image function is defined as the zero-lag cross-correlation of the upgoing and the downgoing waves.

Wavefield extrapolation

The first step in depth migration is to reconstruct the wavefield at all times and all locations within the volume V to be imaged. It is well known (Morse and Feshbach 1953; Berkhout 1985) and it is shown by (A21) that the pressure can be synthesized by means of a monopole and a dipole distribution on the surface S, enclosing V. The strength of each monopole is given by the normal derivative of the pressure field on S. The strength of each dipole is given by the pressure field on S. Assuming that the source in the experiment is located outside V, the pressure at location $(\mathbf{x}, t)$ is given by the integral representation

$$p(\mathbf{x}, t) = \int_V \mathrm{d}V(\mathbf{x}') \tilde{g}(\mathbf{x}, t \,|\, \mathbf{x}', 0) * [f^{(\mathrm{m})}(\mathbf{x}', t) + f^{(\mathrm{d})}(\mathbf{x}', t)], \tag{4a}$$

where

$$f^{(m)}(\mathbf{x}, t) = \oint_S dS(\xi) n_i \frac{1}{\rho(\xi)} [\partial_i^{\xi} p(\xi, t)] \delta(\mathbf{x} - \xi), \tag{4b}$$

$$f^{(d)}(\mathbf{x}, t) = \oint_S dS(\xi) n_i \frac{1}{\rho(\xi)} p(\xi, t)\, \partial_i \delta(\mathbf{x} - \xi), \tag{4c}$$

$\tilde{g}$ is the adjoint Green's function and n_i is component i of an outward-pointing unit vector orthogonal to the surface S bounding the volume V. The adjoint Green's function is defined in Appendix A. $\tilde{g}$ describes the same process as the Green's function g, but in reverse time order, beginning with the final distribution and going backwards in time to the initial source. The time convolution $(*)$ in (4a) for the time-reversed problem is defined in (A17). The pressure field is assumed to obey the final conditions (A4).

Equation (4a) implies that the use of the scalar wave equation to extrapolate the wavefield backwards in time requires the specification of both the pressure and its normal derivative on S.

As noted in the preceding section, the wavefield extrapolation is not performed using the explicit version of (4a), but by solving the corresponding differential equation with source terms given in (4b) and (4c). In a real seismic experiment it is, of course, not possible to measure the pressure and its normal derivative on the whole of the closed surface S. The data are only acquired on a part of S. In this case the closed surface integrals $\oint_S$ should be replaced by integrals along a part of the surface, $\int_S$. In the numerical examples the acquisition surface is vertically plane (see Fig. 1). The lack of information on the full surface gives rise to spatial aperture effects (Wapenaar *et al.* 1989).

Furthermore, in a VSP experiment it is common to record the particle velocities (that is, v_x and v_z in the 2D situation) in the well. Note that if also the pressure can be recorded at an upper depth level z_0, it will be possible to reconstruct the total pressure field in the well from the v_z component by integrating the equation of motion (A1a) in depth, i.e.

$$p(x, z, t) = p(x, z_0, t) - \partial_t \int_{z_0}^{z} d\zeta \rho(x, \zeta) v_z(x, \zeta, t). \tag{5}$$

The normal derivative of the pressure (in a vertical well) is of course found by taking the time derivative of the v_x component multiplied by the density. Thus, in the acoustic approximation it should, in principle, be possible to gain information about the boundary conditions relevant for use in the scalar wave equation. The density in the borehole is assumed to be found from the density log. In the elastic situation it is, however, not possible to extract the tractions from the particle velocities.

Imaging

The basic model for using the U/D imaging concept of Claerbout (1971) is that the pressure wavefield can be decomposed into upgoing and downgoing waves. Thus, the separation of upgoing waves from downgoing waves is an essential step in

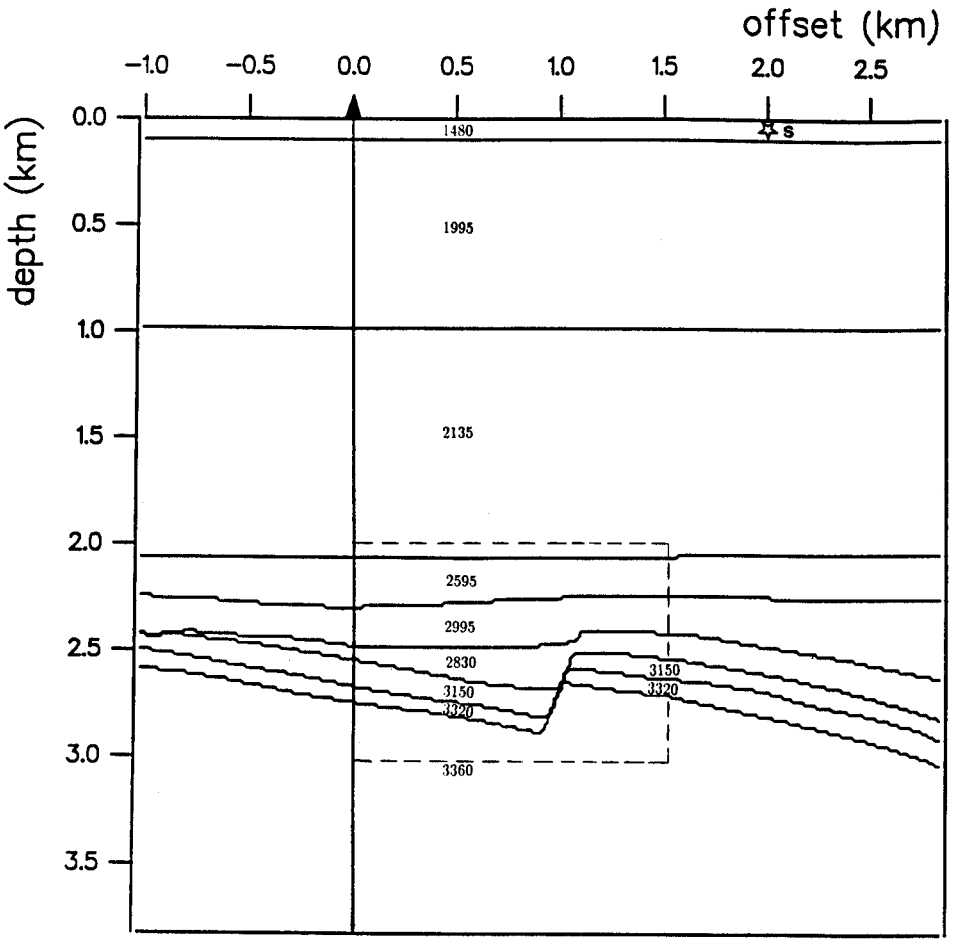

FIG. 1. The velocity model. The well position is at offset 0.0. The source is denoted by S and is located 2 km to the right of the well.

the imaging algorithm. By isolating the two wavefields, their zero-lag cross-correlation can be computed to give information about the image. We use the velocity filter approach as a method for separating the upgoing and downgoing waves (Treitel, Shanks and Frasier 1967). Related techniques have been used with good results (Seeman and Horowicz 1983; Suprajitno and Greenhalgh 1985).

For every lateral position into the target zone, the extrapolated VSP record is transformed into the wavenumber–frequency ($k_z - f$) domain, where events can be identified according to their apparent phase velocities. A downgoing wave in $k_z - f$ space will be characterized as a mode with apparent vertical phase velocity

$$V_{\text{app}} = \frac{\Delta z}{\Delta t} = \frac{f}{k_z}. \tag{6}$$

An upgoing wave has opposite dip compared to a downgoing wave in $z-t$ space, and so the phase velocity of the downgoing wave has a negative sign in $k_z - f$ space. Thus, the upgoing and the downgoing waves are separated into two different quadrants of $k_z - f$ space. The ideal separation filter will be a zero-phase rectangular window which passes only positive or negative wavenumbers. In reality, the filter is gradually tapered in the cut-off area to avoid truncation effect.

The most straightforward way to implement the U/D image concept of Claerbout (1971) is to compute the zero-lag cross-correlation of the upgoing and downgoing waves in the frequency domain:

$$\mathscr{I}_M(\mathbf{x}) = \int_0^T \mathrm{d}t u(\mathbf{x}, t)\, \mathrm{d}(\mathbf{x}, t)$$
$$= \frac{1}{2\pi} \int_{-\omega_N}^{\omega_N} \mathrm{d}\omega U(\mathbf{x}, \omega) D^*(\mathbf{x}, \omega), \tag{7}$$

where $\omega = 2\pi f$ and $\omega_N = \pi/\Delta t$ is the Nyquist frequency. The asterisk (*) denotes a complex conjugate. Equation (7) is a stable approximation to a U/D deconvolution algorithm, and corresponds to matched filtering. The cross-correlation procedure in (7) gives a more low-frequency imaging than the image obtainable using a U/D deconvolution algorithm. Note also that with this equation, the imaging function $\mathscr{I}_M$ will be large where the illumination from the seismic experiment is good and small where the illumination is poor. An advantage of this imaging algorithm is that it does not require any forward-modelling step, and thus the source time function need not to be known. Naturally, this concept has several defects. For instance, diffractions are not correctly treated in the imaging. Also a false image is produced when the U- and D-waves are in-phase, but not on interfaces. However, these defects turn out to be of minor importance. For imaging transmission data, such as offset VSP data, it is the direct wave and its first reflections that give the main contribution to the image. In considering the application of this migration algorithm to real recorded data, the algorithm should be generalized to include elastic wave propagation effects.

Depth Imaging Based on Non-Linear Inversion

The goal of seismic inversion is to estimate earth parameters from measured seismic data. This is done formally by minimizing the least-squares objective function

$$F(\mathbf{m}) = \frac{1}{2} \int_0^T \mathrm{d}t \int_S \mathrm{d}S(\xi)[\Delta p(\xi, t)]^2 \tag{8}$$

with respect to the model parameters $\mathbf{m} = [\mathbf{M}^T, \boldsymbol{\rho}^T]^T$. The objective function measures, in a least-squares sense, the misfit Δp between the measured data (the seismic response of the medium) and the theoretically predicted data obtained from the solution of the wave equation for a given model.

In the numerical examples we assume, for simplicity, that the density is constant. Then the objective function (8) is minimized with respect to the bulk modulus $\mathbf{M}$

only. The model parameter updates are taken in the steepest descent direction

$$\Delta M(\mathbf{x}) = -\alpha \gamma_M(\mathbf{x}), \tag{9}$$

where α is a constant factor and $\gamma_M(\mathbf{x})$ is the gradient of F. We only consider the first iteration in this iterative inversion scheme.

Wavefield extrapolation

In Appendix B (equation (B12a), see also Lailly (1984) and Tarantola (1984)), we show that the gradient of the objective function with respect to the bulk modulus is

$$\gamma_M(\mathbf{x}) = -\frac{1}{M^2(\mathbf{x})} \int_0^T \mathrm{d}t[\partial_t p(\mathbf{x}, t)][\partial_t \phi(\mathbf{x}, t)]. \tag{10}$$

Here the wavefield p represents the forward-propagated predicted pressure field in the background model $M(\mathbf{x})$, and is computed by solving the scalar wave equation (1) with zero initial conditions and the correct source function. The wavefield ϕ is given by (see (B11a))

$$\phi(\mathbf{x}, t) = \int_V \mathrm{d}V(\mathbf{x}') \tilde{g}(\mathbf{x}, t \,|\, \mathbf{x}', 0) * \Delta f^{(\mathrm{m})}(\mathbf{x}', t), \tag{11a}$$

where

$$\Delta f^{(\mathrm{m})}(\mathbf{x}, t) = \int_S \mathrm{d}S(\boldsymbol{\xi})\, \Delta p(\boldsymbol{\xi}, t) \delta(\mathbf{x} - \boldsymbol{\xi}) \tag{11b}$$

and

$$\begin{aligned} \phi(\mathbf{x}, t) &= 0 \qquad t > T, \\ \partial_t \phi(\mathbf{x}, t) &= 0 \qquad t > T. \end{aligned} \tag{11c}$$

The time convolution ($*$) for the time-reversed problem is defined in (A17). Thus, ϕ is a residual wavefield, obtained by applying the difference between the predicted wavefield and the observed wavefield as a source term in the scalar wave equation running backwards in time. The source term consists of a distribution of monopole sources.

Note that $\tilde{g}$ in (11a) represents the adjoint Green's function in the background model. This differs from migration, where the adjoint Green's function, in principle, should propagate in the exact or true medium, that is, in the same medium as the recorded wavefield. However, when the background model in migration is close to the true medium the adjoint Green's function describes the main propagation effects in the true medium. The scattering effects related to the differences in the background and the true medium are ignored. In the case when the contrasts are significant, the migration should be iterative.

Imaging

Our main interest is not to find an estimate of the bulk modulus (or velocity), instead we concentrate on the locations of the interfaces in the subsurface. Having

found the forward-propagated predicted pressure field p and the backward-propagated residual field ϕ, we compute the correlation between their time derivatives to find where the background model should be modified. We then have the following imaging equation

$$\mathscr{I}(\mathbf{x}) = \int_0^T \mathrm{d}t[\partial_t p(\mathbf{x}, t)][\partial_t \phi(\mathbf{x}, t)], \tag{12}$$

'derived' from the theory of acoustic inversion. Compared to the imaging equation (7) for the migration problem we see that (12) contains two time derivatives. The effect of a time derivative is to enhance the high-frequency content in the image.

Note that $\mathscr{I}(\mathbf{x})$ is no longer an expression for the bulk modulus gradient. We have ignored the factor $(-1/M^2(\mathbf{x}))$, as its effect is to enhance the background information in the image (unless it is constant, as in the frst numerical example). We will also apply a spatial filter C to $\mathscr{I}$. The filter removes the low vertical wavenumbers of the image, and is designed in the wavenumber domain. This means that only the high-frequency part of the model perturbations will be shown. The final inversion imaging equation is then

$$\mathscr{I}_I(\mathbf{x}) = \int_V \mathrm{d}V(\mathbf{x}')C(\mathbf{x}, \mathbf{x}')\mathscr{I}(\mathbf{x}'). \tag{13}$$

A fact that will complicate the use of this algorithm on real data, is that the source time function must be known. Furthermore, a modelling algorithm that includes elastic wave propagation effects and gives the correct 3D geometrical spreading should be used to simulate the VSP experiment correctly.

Numerical Results

We present depth imaging from a synthetic VSP section to see what information the algorithms can give about the geology of a fairly complicated structure. The model in Fig. 1 is an example of the geological structure of a North Sea reservoir, obtained by interpreting surface seismic data. The velocities are found from a calibrated borehole compensated sonic log in the area. Note that there is a negative velocity contrast from layer five to layer six. The velocities in the two lowest layers are almost the same, thus we do not expect that their interface will be resolved in the imaging procedure.

The model is approximately 3.8×3.8 km^2 and is composed of faulted layers underlying horizontally layered structures. The source is located 2 km to the right of the well. The subsurface of interest for imaging is marked in Fig. 1 with a dashed line. The VSP data from this model are shown in Fig. 2. Due to the strong reverberations in the first layer we have zeroed the corresponding traces for scaling purposes. The record length is 4.1 s, the sampling interval in time is 1 ms, and the geophone (grid) spacing is 15 m. The source wavelet is assumed to be known in the inversion imaging; it has a dominant frequency of 30 Hz.

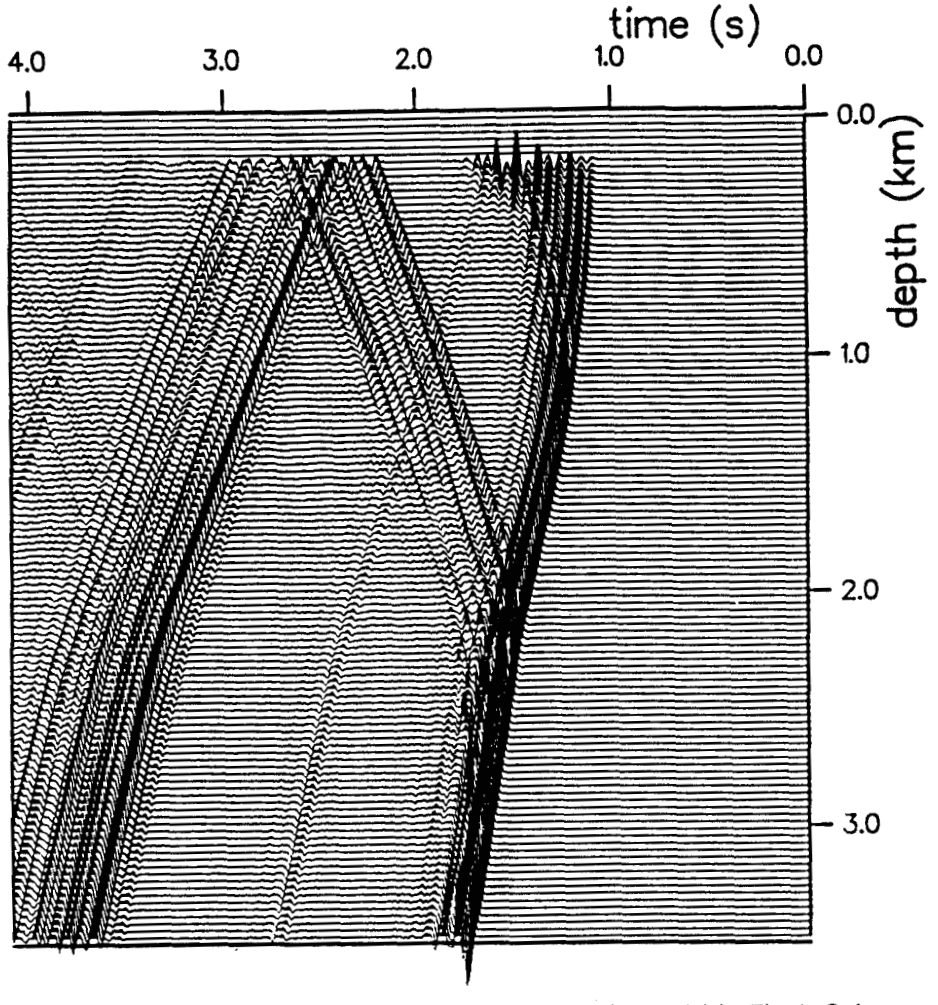

FIG. 2. The reference VSP data corresponding to the velocity model in Fig. 1. Only every second trace is plotted. The first six traces are zeroed for scaling purposes.

To test the sensitivity of the two imaging algorithms to errors in the velocity model, we conduct tests on the following models.

1. We assume that the velocities in layer 1, 2, 3 and 4 are known, and in the rest of the layers we use the same velocities as in layer 4. That is, from a depth of approximately 2.1 km the velocity is constant.
2. We assume a model consisting of plane horizontal layers, having the correct depth and velocities in the well position. Also in this example, the subsurface above the target zone is fully known.

It is important that a good macromodel containing low wavenumber information in the velocity distribution is available above the target zone. Such a macromodel may

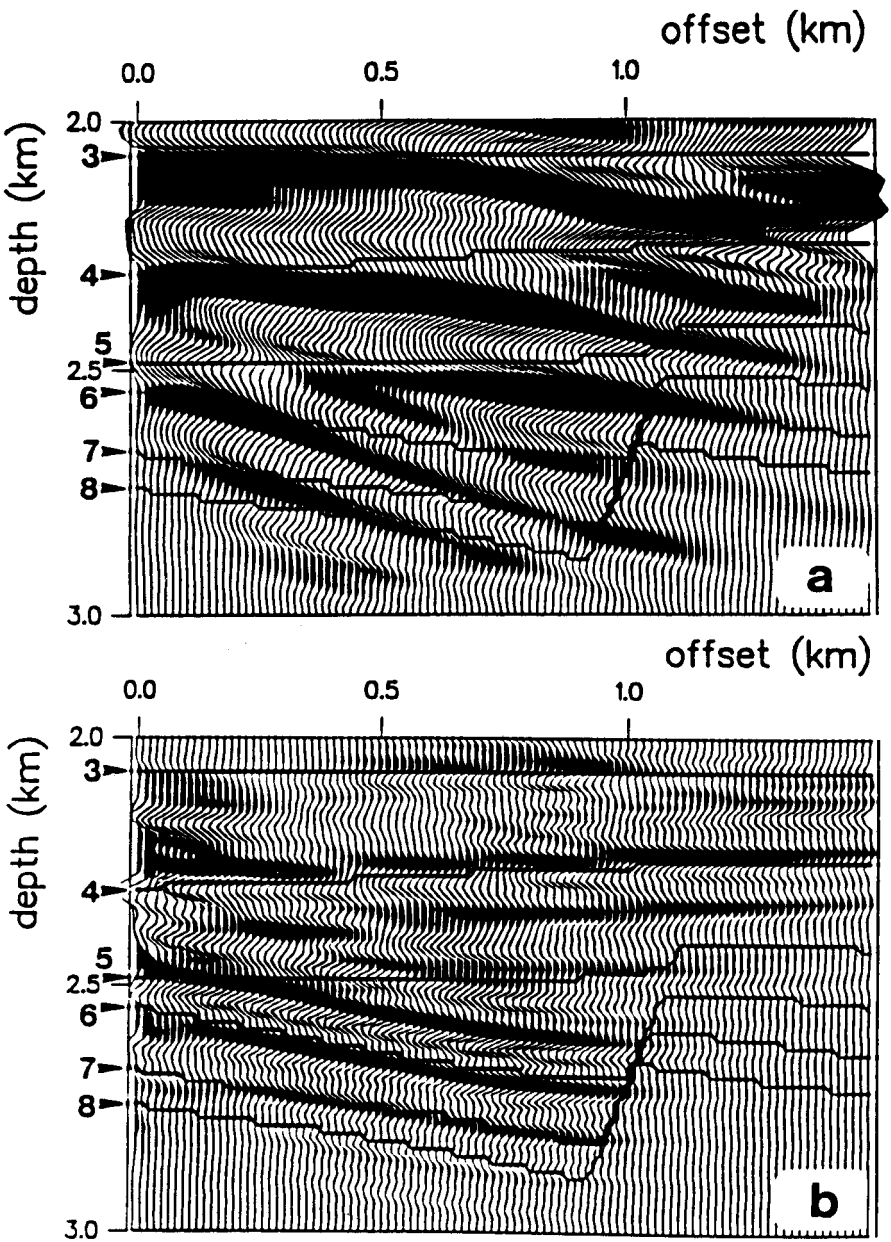

FIG. 3. Depth image using a background model with velocities constant from depth 2.1 km and below. The true model is superimposed. The reflector positions are marked with an arrow. (a) U/D imaging; (b) inversion imaging.

be obtained using, for instance, traveltime tomography, and will eliminate the propagation effects of the strong first arrival above the target.

In Fig. 3 we show the results from the first test. The true interface positions are superimposed on this and the subsequent plots. The layer interfaces in the well are numbered and their positions marked with an arrow. The image using the U/D concept (Fig. 3a) is not comparable with the true structural trends. However, a reasonable image is obtained close to the well. As the field is extrapolated away from the well, the imaging gives reflector positions that are progressively more in error. The discrepancy between this depth image and the true depth image is due to the very large difference between the background model and the true model.

The image obtained by using the true velocity model in the migration will of course be much better. In this case, as shown in Fig. 4, the greater part of the medium is recovered. The presence of the fault is indicated by a change in the image in this area. We do not expect that reflectors to the right of the fault can be imaged, as almost no energy from these layers is measured in the well. We observe that the sign of reflector five is negative, because the upgoing and downgoing waves at this reflector are of opposite polarity. Also, a false reflector image crosses the horizontal reflector five. This false image is created by the correlation of an upgoing wave and a surface-reverberated downgoing wave.

In Fig. 3b we show the image based on the inversion algorithm. The residual source wavefield in the well for this example is shown in Fig. 5. Observe that the strong direct arrival does not contribute to the residual above the target zone. A filter that removes the low vertical wavenumbers is applied in the imaging equation

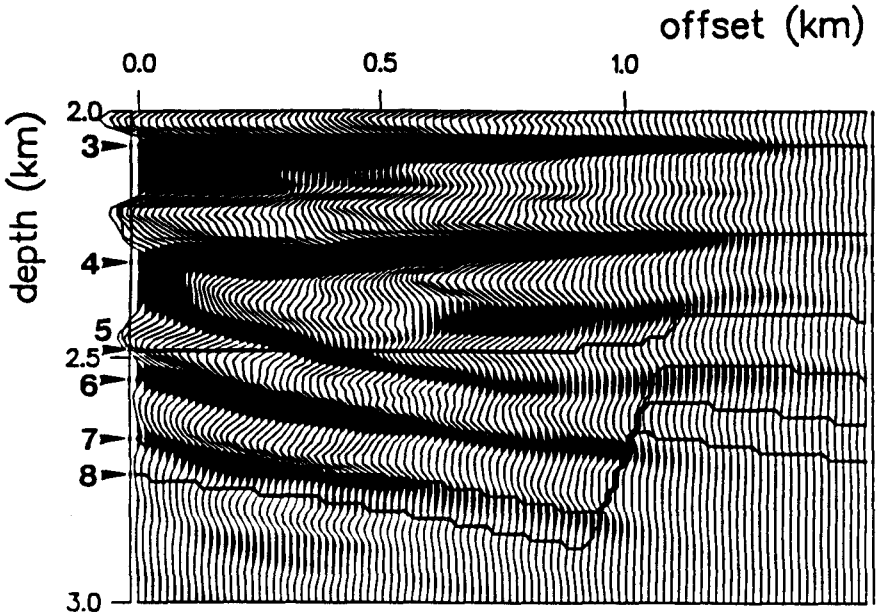

FIG. 4. Depth image with the U/D concept using the true velocity model. The true model is superimposed. The reflector positions are marked with an arrow.

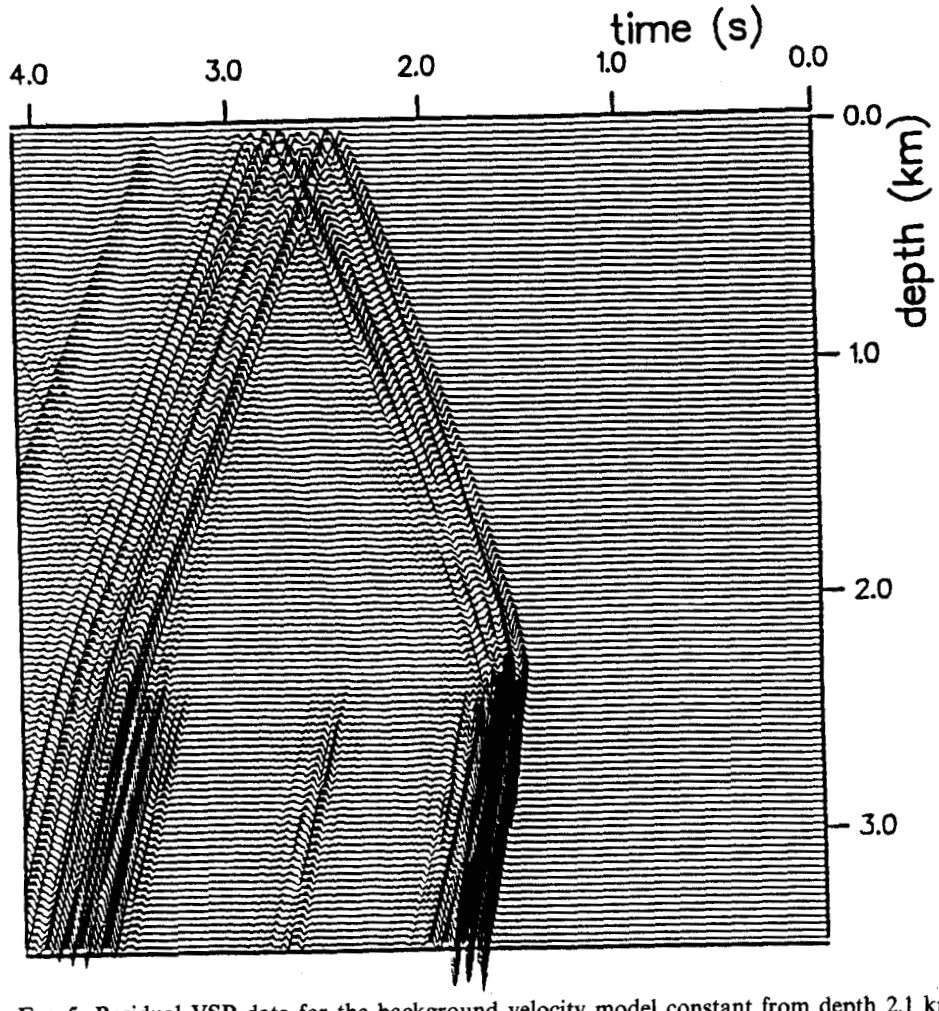

FIG. 5. Residual VSP data for the background velocity model constant from depth 2.1 km. Only every second trace is plotted.

(13). This means that only the high-frequency part of the model perturbations is shown. The position of reflector four is nearly recovered. Note that only information about the first three interfaces was given in the background velocity model. The negative sign of reflector five can be followed to some degree, but is much distorted by the false image between interfaces five and six. This false reflector image was also seen in the image in Fig. 4. The general structural trends of interfaces six and seven are consistent with the model. Note that the character of the image changes in the fault plane, indicating the presence of the fault.

The inversion image is quite acceptable, considering that only one shot is used and that the error between the true velocity model and the background velocity

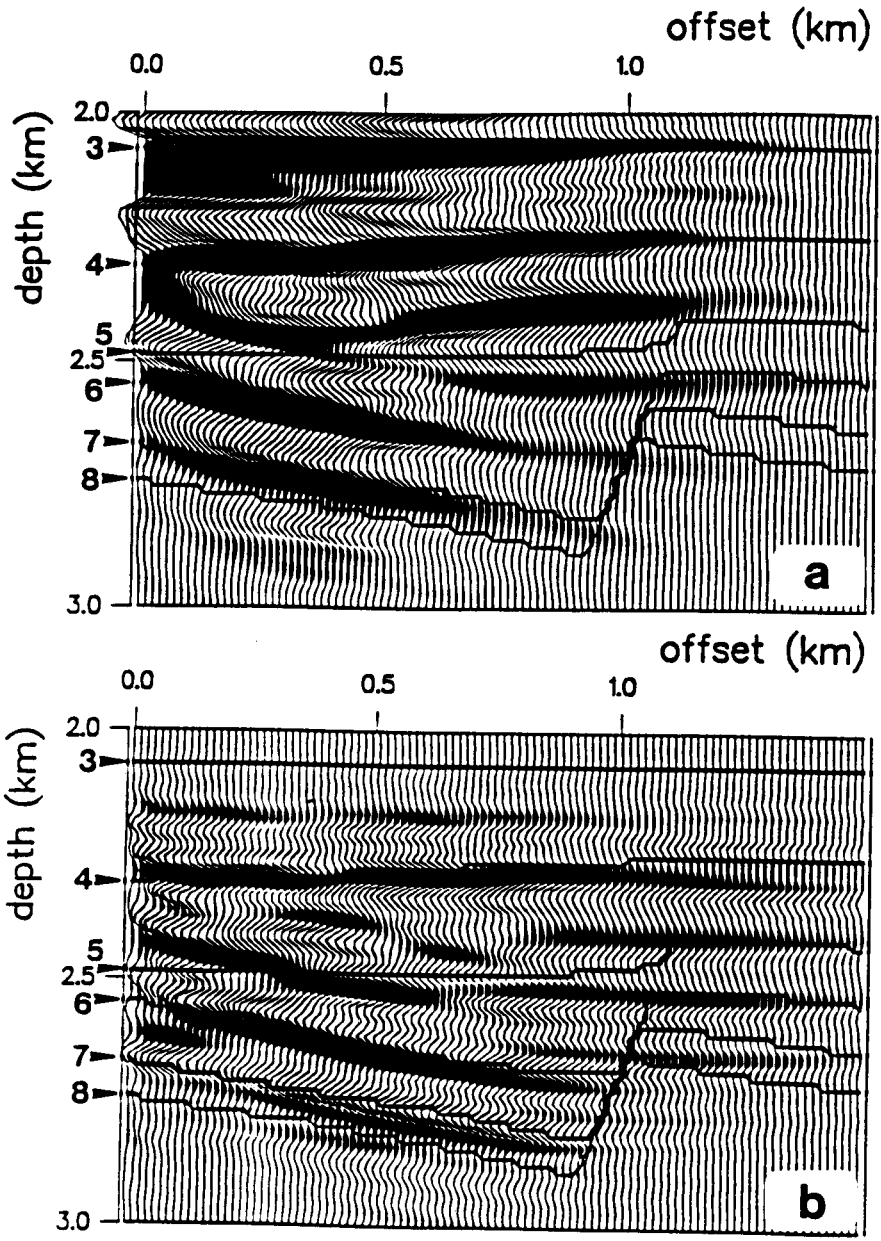

FIG. 6. Depth image using a plane horizontally layered background velocity model, with layers having the correct depth and velocity in the well. The true model is superimposed. The reflector positions are marked with an arrow. (a) U/D imaging; (b) inversion imaging.

model is quite large. The image reconstruction is, of course, determined by the receiver array configuration and the source location. The partial image obtained from this minimal amount of data is encouraging. This processing scheme is comparable to processing of surface seismic prestack data from a single shot. Multiple-offset VSP data should be used to obtain the additional information necessary for obtaining a clearer image.

In Fig. 6 we show the results from the second test, using a plane horizontally layered background velocity model, with layers that have the correct depth and velocity in the well. Figure 6a shows the result using the U/D imaging algorithm. Compared to the previous example using the U/D imaging concept, the image reconstruction is good: interfaces three to five are recovered. However, for these reflectors the background model is consistent with the true model. Also, the trends of reflectors six and seven are indicated. This example underlines the importance of having a good background velocity model in depth migration.

Finally, in Fig. 6b we show the image using the inversion algorithm. Once again some of the structural trends are recovered. Starting with an assumption of plane horizontal layers, the algorithm partly restores, in one iteration, layer interfaces with approximately the correct dip. To some degree we can trace the fault plane, indicated by the vanishing of the two last reflectors from the bottom. Note that we are constructing an image proportional to the velocity perturbations, thus we will observe some of the plane layer background velocity model. The inversion algorithm tries to rectify the erroneous interfaces in the background model. This is most clearly seen on the false reflector image running through the fault plane.

Conclusions

We have compared two depth imaging algorithms for offset VSP data. The first one is based on the U/D imaging concept, and requires a reasonable knowledge of the velocity distribution at all subsurface positions for a successful application. The deviation between the true and imaged reflectors in the target zone increased away from the well.

Replacing the migration equations with the equations of inversion seems to be a good strategy for the depth imaging of offset VSP data. In the first example, imaging based on inversion theory was much more successful than imaging based on the U/D concept. In the second example the images gave nearly the same information. However, the inversion image contains more high frequencies due to the time derivatives appearing in (12). A reasonable image of the target region was constructed from only one shot. For the delineation of such a complicated structure as in this example, multiple offsets are important.

Spatial aperture effects in the algorithms were not investigated.

Acknowledgements

We thank Eivind Berg for supplying us with the velocity model used in the numerical examples, and Olav Holberg for the excellent design of the finite-difference operators used in the computations. We are grateful for stimulating discussions with the SU(5) members Jan Helgesen and Martin Landrø at IKU.

APPENDIX A

The acoustic equations

The material in Appendix A is well-known, but we include it for completeness. An excellent book for readers seeking more details is Morse and Feshbach (1953). The following material relies heavily on this source.

The system of equations governing the wave motion consists of the equation of motion and the pressure–displacement relation (Hooke's law),

$$\rho(\mathbf{x})\partial_t^2 u_i(\mathbf{x}, t) = -\partial_i p(\mathbf{x}, t) + f_i(\mathbf{x}, t), \tag{A1a}$$

$$p(\mathbf{x}, t) = -M(\mathbf{x})\, \partial_i u_i(\mathbf{x}, t), \tag{A1b}$$

where p is the pressure, u_i is the ith displacement component, f_i is the ith component of the body-force distribution, ρ is the density, M is the bulk modulus and $\mathbf{x}$ is a shorthand notation for the Cartesian coordinates. The two first-order partial differential equations (A1a) and (A1b) can be combined into the scalar wave equation for pressure

$$\left[\frac{1}{M(\mathbf{x})}\,\partial_t^2 - \partial_i \frac{1}{\rho(\mathbf{x})}\,\partial_i\right] p(\mathbf{x}, t) = f(\mathbf{x}, t), \tag{A2a}$$

where

$$f(\mathbf{x}, t) = -\partial_i \frac{1}{\rho(\mathbf{x})}\, f_i(\mathbf{x}, t). \tag{A2b}$$

The pressure may obey initial conditions

$$\begin{aligned} p(\mathbf{x}, t) &= 0 \qquad t < 0, \\ \partial_t p(\mathbf{x}, t) &= 0 \qquad t < 0, \end{aligned} \tag{A3}$$

or final conditions

$$\begin{aligned} p(\mathbf{x}, t) &= 0 \qquad t > T, \\ \partial_t p(\mathbf{x}, t) &= 0 \qquad t > T, \end{aligned} \tag{A4}$$

where the time T is constrained to be greater than the duration of the seismic response.

The Green's function for the scalar wave equation

The equation determining the Green's function is

$$\left[\frac{1}{M(\mathbf{x})}\,\partial_t^2 - \partial_i \frac{1}{\rho(\mathbf{x})}\,\partial_i\right] g(\mathbf{x}, t \mid \mathbf{x}', t') = \delta(\mathbf{x} - \mathbf{x}')\delta(t - t'). \tag{A5}$$

The Green's function satisfies the causality condition

$$g(\mathbf{x}, t \mid \mathbf{x}', t') = 0 \quad \text{if} \quad t < t',$$

$$\partial_t g(\mathbf{x}, t \mid \mathbf{x}', t') = 0 \quad \text{if} \quad t < t', \tag{A6}$$

is invariant with respect to time translation (medium parameters are independent of time)

$$g(\mathbf{x}, t \mid \mathbf{x}', t') = g(\mathbf{x}, t + \tau \mid \mathbf{x}', t' + \tau), \tag{A7}$$

and, assuming homogeneous boundary conditions, the space–time reciprocity relationship

$$g(\mathbf{x}, t \mid \mathbf{x}', t') = g(\mathbf{x}', -t' \mid \mathbf{x}, -t) \tag{A8}$$

is obtained.

The adjoint Green's function $\tilde{g}$ describes the same process as the Green's function g, but in reverse time order, beginning with the final distribution and going backwards in time to the initial source. The adjoint Green's function is defined by the relationship

$$g(\mathbf{x}, -t \mid \mathbf{x}', -t') = \tilde{g}(\mathbf{x}, t \mid \mathbf{x}', t'), \tag{A9}$$

and $\tilde{g}$ satisfies the time-reversed equation

$$\left[\frac{1}{M(\mathbf{x})}\,\partial_t^2 - \partial_i \frac{1}{\rho(\mathbf{x})}\,\partial_i\right]\tilde{g}(\mathbf{x}, t \mid \mathbf{x}', t') = \delta(\mathbf{x} - \mathbf{x}')\delta(t - t'). \tag{A10}$$

Condition (A6) is replaced by

$$\tilde{g}(\mathbf{x}, t \mid \mathbf{x}', t') = 0 \quad \text{if} \quad t > t',$$

$$\partial_t \tilde{g}(\mathbf{x}, t \mid \mathbf{x}', t') = 0 \quad \text{if} \quad t > t'. \tag{A11}$$

Relation (A8) now reads

$$g(\mathbf{x}, t \mid \mathbf{x}', t') = \tilde{g}(\mathbf{x}', t' \mid \mathbf{x}, t). \tag{A12}$$

Representation theorems for the pressure

The integral solution of the inhomogeneous scalar wave equation (A2a) in terms of the Green's function g assuming initial conditions (A3) for the pressure is (Morse and Feshbach 1953)

$$\begin{aligned} p(\mathbf{x}, t) = &\int_V \mathrm{d}V(\mathbf{x}')g(\mathbf{x}, t \mid \mathbf{x}', 0) * f(\mathbf{x}', t) \\ &+ \oint_S \mathrm{d}S(\boldsymbol{\xi})n_i \frac{1}{\rho(\boldsymbol{\xi})}\,[g(\mathbf{x}, t \mid \boldsymbol{\xi}, 0) * \partial_i^{\xi} p(\boldsymbol{\xi}, t) \\ &- p(\boldsymbol{\xi}, t) * \partial_i^{\xi} g(\mathbf{x}, t \mid \boldsymbol{\xi}, 0)], \end{aligned} \tag{A13}$$

where the convolution operator $(*)$ is defined by

$$a(t) * b(t) = \int_{-\infty}^{t} \mathrm{d}t' a(t - t')b(t'), \tag{A14}$$

and n_i is component i of an outward-pointing unit vector orthogonal to the recording surface S bounding the volume V. We have used the shorthand notation ∂_i^{ξ} for indicating that the derivative is to be taken with respect to the coordinate ξ on S. The normal gradients are taken in the outward direction. In the case of homogeneous boundary conditions for the Green's function and the pressure, the integral representation (A13) becomes

$$p(\mathbf{x}, t) = \int_V \mathrm{d}V(\mathbf{x}') g(\mathbf{x}, t \,|\, \mathbf{x}', 0) * f(\mathbf{x}', t) \tag{A15}$$

The wave equation is symmetric with respect to time. This implies that the closed-form integral solution of the inhomogeneous scalar wave equation (A2a) in terms of the adjoint Green's function invoking final conditions (A4) for the pressure is (Morse and Feshbach 1953)

$$\begin{aligned} p(\mathbf{x}, t) = & \int_V \mathrm{d}V(\mathbf{x}') \tilde{g}(\mathbf{x}, t \,|\, \mathbf{x}', 0) * f(\mathbf{x}', t) \\ & + \oint_S \mathrm{d}S(\xi) n_i \frac{1}{\rho(\xi)} [\tilde{g}(\mathbf{x}, t \,|\, \xi, 0) * \partial_i^{\xi} p(\xi, t) \\ & - p(\xi, t) * \partial_i^{\xi} \tilde{g}(\mathbf{x}, t \,|\, \xi, 0)], \end{aligned} \tag{A16}$$

where the convolution operator (*) now is defined by

$$\tilde{a}(t) * b(t) = \int_t^T \mathrm{d}t' \tilde{a}(t - t') b(t'). \tag{A17}$$

The first integral in (A16) represents the effects of sinks (inverse sources). The second integral represents the effects of boundary conditions. Equation (A16) illustrates that the Green's function is a scalar kernel of an integral operator which transforms the source density and boundary conditions into the solution.

The final conditions (A4) for the pressure will, in practice, be non-zero for the volume covered by the seismic experiment. Since we are not able to measure this information, we must therefore set the final conditions to zero. The reconstruction of the pressure is, incorrectly, only based on the surface integral (containing measurable quantities).

In a real seismic experiment it is, of course, not possible to measure the pressure and its normal derivative on the whole of the closed surface S. The fields are only acquired on a part of S. In this case the closed surface integrals $\oint_S$ should be replaced by integrals along a part of the surface, $\int_S$. The lack of information on the full surface gives rise to spatial aperture effects.

Body-force equivalents

We shall use the fact that boundary conditions on a surface are equivalent to source distributions on the surface. The first part of the surface integral in (A16) can

be written as

$$\oint_S dS(\xi) n_i \frac{1}{\rho(\xi)} \tilde{g}(\mathbf{x}, t \mid \xi, 0) * \partial_i^{\xi} p(\xi, t)$$

$$= \int_V dV(\mathbf{x}') \tilde{g}(\mathbf{x}, t \mid \mathbf{x}', 0) * f^{(m)}(\mathbf{x}', t), \tag{A18a}$$

where

$$f^{(m)}(\mathbf{x}, t) = \oint_S dS(\xi) n_i \frac{1}{\rho(\xi)} [\partial_i^{\xi} p(\xi, t)] \delta(\mathbf{x} - \xi). \tag{A18b}$$

Using

$$\partial_i^{\xi} \tilde{g}(\mathbf{x}, t \mid \xi, 0) = - \int_V dV(\mathbf{x}') [\partial_i' \delta(\mathbf{x}' - \xi)] \tilde{g}(\mathbf{x}, t \mid \mathbf{x}', 0), \tag{A19}$$

the second part of the surface integral in (A16) becomes

$$\oint_S dS(\xi) n_i \frac{1}{\rho(\xi)} p(\xi, t) * \partial_i^{\xi} \tilde{g}(\mathbf{x}, t \mid \xi, 0)$$

$$= - \int_V dV(\mathbf{x}') \tilde{g}(\mathbf{x}, t \mid \mathbf{x}', 0) * f^{(d)}(\mathbf{x}', t). \tag{A20a}$$

where

$$f^{(d)}(\mathbf{x}, t) = \oint_S dS(\xi) n_i \frac{1}{\rho(\xi)} p(\xi, t) \partial_i \delta(\mathbf{x} - \xi). \tag{A20b}$$

Thus, (A16) can be written as

$$p(\mathbf{x}, t) = \int_V dV(\mathbf{x}') \tilde{g}(\mathbf{x}, t \mid \mathbf{x}', 0) * [f(\mathbf{x}', t) + f^{(m)}(\mathbf{x}', t) + f^{(d)}(\mathbf{x}', t)]. \tag{A21}$$

Equation (A21) demonstrates that the pressure field at a coordinate $(\mathbf{x}, t)$ in the volume V may be synthesized by means of sinks in V and a monopole and a dipole distribution on the surface S, enclosing V. The strength of each monopole is given by the normal derivative of the pressure on S. The strength of each dipole is given by the pressure field on S.

APPENDIX B

The gradient of the objective function

We give a short summary of the mathematics of the inversion theory given by Lailly (1984) and Tarantola (1984). For completeness, we give the gradients both

with respect to the bulk modulus and density even though in the numerical examples we use constant density for simplicity.

We consider the objective function (8) for one shot position

$$F(\mathbf{m}) = \frac{1}{2}\int_0^T \mathrm{d}t \int_S \mathrm{d}S(\xi)[\Delta p(\xi, t)]^2, \tag{B1}$$

where the model vector is $\mathbf{m} = [\mathbf{M}^T, \boldsymbol{\rho}^T]^T$ and $\Delta p = p - p^{\mathrm{obs}}$ is the residual pressure component on S. Note that the surface integral now need not be closed: S denotes the receiver surface.

In order to perform inversion using a steepest descent algorithm, the gradient of the objective function with respect to the model parameters is required. In continuous form, the gradient with respect to the model parameter $m(\mathbf{x})$ is

$$\gamma_m(\mathbf{x}) = \int_0^T \mathrm{d}t \int_S \mathrm{d}S(\xi) K_m(\xi, t; \mathbf{x}) \Delta p(\xi, t), \tag{B2}$$

that is, the integral over the data space of the data perturbations (residuals) multiplied by the Fréchet kernel

$$K_m(\xi, t; \mathbf{x}) = \frac{\partial p(\xi, t)}{\partial m(\mathbf{x})}. \tag{B3}$$

The Fréchet kernel may be computed from the linearized forward problem, which has the continuous form

$$\Delta p(\xi, t) = \int_V \mathrm{d}V(\mathbf{x}) K_m(\xi, t; \mathbf{x}) \Delta m(\mathbf{x}), \tag{B4}$$

that is, the integral over the model space of the model perturbations $\Delta m(\mathbf{x})$ multiplied by the Fréchet kernel. Equation (B4) shows that perturbations in the model parameters lead to a perturbation in the field.

The scalar wave equation is given in (A2a). A perturbation of the model parameters,

$$M(\mathbf{x}) \to M(\mathbf{x}) + \Delta M(\mathbf{x}),$$

$$\rho(\mathbf{x}) \to \rho(\mathbf{x}) + \Delta\rho(\mathbf{x}),$$

gives a perturbation of the pressure field,

$$p(\mathbf{x}, t) \to p(\mathbf{x}, t) + \Delta p(\mathbf{x}, t).$$

Neglecting higher-order terms, the pressure residuals are given by the equation

$$\left[\frac{1}{M(\mathbf{x})}\partial_t^2 - \partial_j \frac{1}{\rho(\mathbf{x})}\partial_j\right]\Delta p(\mathbf{x}, t)$$

$$= \frac{\Delta M(\mathbf{x})}{M^2(\mathbf{x})}\partial_t^2 p(\mathbf{x}, t) - \partial_j \frac{\Delta\rho(\mathbf{x})}{\rho^2(\mathbf{x})}\partial_j p(\mathbf{x}, t), \tag{B5a}$$

with initial conditions

$$\Delta p(\mathbf{x}, t) = 0 \qquad t < 0,$$
$$\partial_t \Delta p(\mathbf{x}, t) = 0 \qquad t < 0. \tag{B5b}$$

The solution of (B5a) at the receiver positions ξ in terms of the Green's function is (in analogy with (A2a) and (A15))

$$\begin{aligned}\Delta p(\xi, t) &= \int_V \mathrm{d}V(\mathbf{x}) g(\xi, t \mid \mathbf{x}, 0) \\ &\quad * \left\{ \frac{\Delta M(\mathbf{x})}{M^2(\mathbf{x})} \partial_t^2 p(\mathbf{x}, t) - \partial_j \frac{\Delta \rho(\mathbf{x})}{\rho^2(\mathbf{x})} \partial_j p(\mathbf{x}, t) \right\} \\ &= \int_V \mathrm{d}V(\mathbf{x}) g(\xi, t \mid \mathbf{x}, 0) * \frac{1}{M^2(\mathbf{x})} \partial_t^2 p(\mathbf{x}, t) \Delta M(\mathbf{x}) \\ &\quad + \int_V \mathrm{d}V(\mathbf{x}) [\partial_j g(\xi, t \mid \mathbf{x}, 0)] * \frac{1}{\rho^2(\mathbf{x})} [\partial_j p(\mathbf{x}, t)] \Delta \rho(\mathbf{x}).\end{aligned} \tag{B6}$$

Equation (B6) defines the Fréchet kernels to be used in the adjoint state:

$$K_M(\xi, t; \mathbf{x}) = \frac{1}{M^2(\mathbf{x})} g(\xi, t \mid \mathbf{x}, 0) * \partial_t^2 p(\mathbf{x}, t), \tag{B7a}$$

$$K_\rho(\xi, t; \mathbf{x}) = \frac{1}{\rho^2(\mathbf{x})} [\partial_j g(\xi, t \mid \mathbf{x}, 0)] * [\partial_j p(\mathbf{x}, t)]. \tag{B7b}$$

Inserting the above kernels in (B2) gives

$$\gamma_M(\mathbf{x}) = \frac{1}{M^2(\mathbf{x})} \int_0^T \mathrm{d}t \int_S \mathrm{d}S(\xi) g(\xi, t \mid \mathbf{x}, 0) * [\partial_t^2 p(\mathbf{x}, t)] \Delta p(\xi, t), \tag{B8a}$$

$$\gamma_\rho(\mathbf{x}) = \frac{1}{\rho^2(\mathbf{x})} \int_0^T \mathrm{d}t \int_S \mathrm{d}S(\xi) [\partial_j g(\xi, t \mid \mathbf{x}, 0)] * [\partial_j p(\mathbf{x}, t)] \Delta p(\xi, t). \tag{B8b}$$

By changing the order of the time integrations, interchanging t and t', and using the properties of the Green's function, we find that

$$\begin{aligned}\gamma_M(\mathbf{x}) &= \frac{1}{M^2(\mathbf{x})} \int_0^T \mathrm{d}t [\partial_t^2 p(\mathbf{x}, t)] \int_{t-\varepsilon}^T \mathrm{d}t' \\ &\quad \times \int_S \mathrm{d}S(\xi) g(\mathbf{x}, -t \mid \xi, -t') \Delta p(\xi, t'),\end{aligned} \tag{B9a}$$

$$\begin{aligned}\gamma_\rho(\mathbf{x}) &= \frac{1}{\rho^2(\mathbf{x})} \int_0^T \mathrm{d}t [\partial_j p(\mathbf{x}, t)] \partial_j \int_{t-\varepsilon}^T \mathrm{d}t' \\ &\quad \times \int_S \mathrm{d}S(\xi) g(\mathbf{x}, -t \mid \xi, -t') \Delta p(\xi, t').\end{aligned} \tag{B9b}$$

Introducing the adjoint Green's function and the convolution operator (A17) we have

$$\gamma_M(\mathbf{x}) = \frac{1}{M^2(\mathbf{x})} \int_0^T \mathrm{d}t[\partial_t^2 p(\mathbf{x}, t)] \times \int_S \mathrm{d}S(\xi)\tilde{g}(\mathbf{x}, t \mid \xi, 0) * \Delta\rho(\xi, t), \tag{B10a}$$

$$\gamma_\rho(\mathbf{x}) = \frac{1}{\rho^2(\mathbf{x})} \int_0^T \mathrm{d}t[\partial_j p(\mathbf{x}, t)]\ \partial_j \times \int_S \mathrm{d}S(\xi)\tilde{g}(\mathbf{x}, t \mid \xi, 0) * \Delta p(\xi, t). \tag{B10b}$$

Defining the residual field

$$\phi(\mathbf{x}, t) = \int_S \mathrm{d}S(\xi)\tilde{g}(\mathbf{x}, t \mid \xi, 0) * \Delta p(\xi, t) = \int_V \mathrm{d}V(\mathbf{x}')\tilde{g}(\mathbf{x}, t \mid \mathbf{x}', 0) * \Delta f^{(\mathrm{m})}(\mathbf{x}', t), \tag{B11a}$$

satisfying final conditions

$$\phi(\mathbf{x}, t) = 0 \qquad t > T,$$
$$\partial_t \phi(\mathbf{x}, t) = 0 \qquad t > T, \tag{B11b}$$

and having source term

$$\Delta f^{(\mathrm{m})}(\mathbf{x}, t) = \int_S \mathrm{d}S(\xi)\Delta p(\xi, t)\delta(\mathbf{x} - \xi), \tag{B11c}$$

the gradients of the objective function (B1) are

$$\gamma_M(\mathbf{x}) = -\frac{1}{M^2(\mathbf{x})} \int_0^T \mathrm{d}t[\partial_t p(\mathbf{x}, t)][\partial_t \phi(\mathbf{x}, t)], \tag{B12a}$$

$$\gamma_\rho(\mathbf{x}) = \frac{1}{\rho^2(\mathbf{x})} \int_0^T \mathrm{d}t[\partial_j p(\mathbf{x}, t)][\partial_j \phi(\mathbf{x}, t)]. \tag{B12b}$$

References

Berkhout, A.J. 1985. *Seismic Migration: Imaging of Acoustic Energy by Wavefield Extrapolation. A. Theoretical aspects.* Elsevier Science Publishing Co.

Berkhout, A.J. 1986. Seismic inversion in terms of pre-stack migration and multiple elimination. *Proceedings of the IEEE* **74**, 415–427.

Beylkin, G. and Burridge, R. 1990. Linearised inverse scattering problems in acoustics and elasticity. *Wave Motion* **12**, 15–52.

CHANG, W.F. and MCMECHAN, G.A. 1986. Reverse-time migration of offset vertical seismic profiling data using the excitation-time imaging condition. *Geophysics* **51**, 67–84.

CLAERBOUT, J.F. 1971. Toward a unified theory of reflector mapping. *Geophysics* **36**, 467–481.

DAI, T. and KUO, J.-T. 1986. Real data results of Kirchhoff elastic wave migration. *Geophysics* **51**, 1006–1011.

DILLON, P.B. 1988. Vertical seismic profile migration using the Kirchhoff integral. *Geophysics* **53**, 786–799.

DILLON, P.B. 1990. A comparison between Kirchhoff and GRT migration on VSP data. *Geophysical Prospecting* **38**, 757–777.

DILLON, P.B., AHMED, H. and ROBERTS, T. 1988. Migration of mixed-mode VSP wavefields. *Geophysical Prospecting* **36**, 825–846.

HOLBERG, O. 1987. Computational aspects of the choice of operator and sampling interval for numerical differentiation in large-scale simulation of wave phenomena. *Geophysical Prospecting* **35**, 629–655.

HU, L. and MCMECHAN, G.A. 1986. Migration of VSP data by ray equation extrapolation in 2D variable velocity media. *Geophysical Prospecting* **34**, 704–734.

KEHO, T.H. 1984. Kirchhoff migration for vertical seismic profiles. 54th SEG meeting, Atlanta. Expanded Abstracts, 694–696.

KOHLER, K. and KOENIG, M. 1986. Reconstruction of reflecting structures from vertical seismic profiles with a moving source. *Geophysics* **51**, 1923–1938.

LAILLY, P. 1984. The seismic inverse problem as a sequence of before stack migrations. In: *Inverse Problems of Acoustic and Elastic Waves*. F. Santosa, Y. H. Pao, W. W. Symes, C. Holland (eds), 206–220. Society of Industrial and Applied Mechanics.

MILLER, D., ORISTAGLIO, M. and BEYLKIN, G. 1987. A new slant on seismic imaging: migration and internal geometry. *Geophysics* **52**, 943–964.

MORSE, P.M. and FESHBACH, H. 1953. *Methods of Theoretical Physics*. McGraw–Hill Book Co.

SEEMAN, B. and HOROWICZ, L. 1983. Vertical seismic profiling. Separation of upgoing and downgoing acoustic waves in a stratified medium. *Geophysics* **48**, 555–568.

SUPRAJITNO, M. and GREENHALGH, S.A. 1985. Separation of upgoing and downgoing waves in vertical seismic profiling by contour-slice filtering. *Geophysics* **50**, 950–962.

TARANTOLA, A. 1984. Inversion of seismic reflection data in the acoustic approximation. *Geophysics* **49**, 1259–1266.

TREITEL, S., SHANKS, J.L. and FRASIER, C.W. 1967. Some aspects of fan filtering. *Geophysics* **32**, 789–800.

WAPENAAR, C.P.A., PEELS, G.L., BUDEJICKY, V. and BERKHOUT, A.J. 1989. Inverse extrapolation of primary seismic waves. *Geophysics* **54**, 853–863.

WHITMORE, N.D. and LINES, L.R. 1986. Vertical seismic profiling depth migration of a salt dome flank. *Geophysics* **51**, 1087–1109.

WIGGINS, J.W. 1984. Kirchhoff integral extrapolation and migration of nonplanar data. *Geophysics* **49**, 239–1248.

WIGGINS, J.W. and LEVANDER, A.R. 1984. Migration of multiple offset synthetic vertical seismic profile data in complex structures. In: *Advances in Geophysical Data Processing* **1**, M. Simaan (ed.), 269–289. JAI Press, London.